ACS APPLIED MATERIALS & INTERFACES

www.acsami.org

Research Article

Evaluation of Amorphous Oxide Coatings for High-Voltage Li-Ion Battery Applications Using a First-Principles Framework

Jianli Cheng, Eric Sivonxay, and Kristin A. Persson*

Cite This: https://dx.doi.org/10.1021/acsami.0c10000

Read Online

ACCESS | Metrics & More | Article Recommendations | Supporting Information

ABSTRACT: Cathode surface coatings are widely used industrially as a means to suppress degradation and improve electrochemical performance of lithium-ion batteries. However, developing an optimal coating is challenging, as different coating materials may enhance one aspect of performance while hindering another. To elucidate the fundamental thermodynamic and transport properties of amorphous cathode coating materials, here, we present a framework for calculating and analyzing the Li^+ and O^{2-} transport and the stability against delithiation in such materials. Our framework includes systematic workflows of *ab-initio* molecular dynamics calculations to obtain amorphous structures and diffusion trajectories coupled with an analysis of critical changes of the active-ion local environment during diffusion. Based on these data, we provide an estimate of room-temperature diffusivities, including statistical error bars, and the evaluation of the coating suitability in terms of its ability to facilitate Li^+ transport while blocking O^{2-} transport. Finally, we add the thermodynamic stability analysis of the coating chemistry within the operating voltage of common Li-ion cathodes. We apply this framework to two commonly used amorphous coating materials, Al_2O_3 and ZnO. We find that (1) in general, a higher Li^+ content increases both Li^+ and O^{2-} diffusivities in both Al_2O_3 and ZnO. Also, Li^+ and O^{2-} diffuse much faster in ZnO than in Al_2O_3. (2) However, neither Al_2O_3 nor ZnO is expected to retain a significant concentration of Li^+ at high charge. (3) ZnO performs much more poorly in terms of O^{2-} blocking, and hence, Al_2O_3 is preferred for high-voltage cathode applications. These results will help to quantitatively evaluate amorphous materials, such as metal oxides and fluorides, for different performance metrics and facilitate the development of optimal cathode coatings.

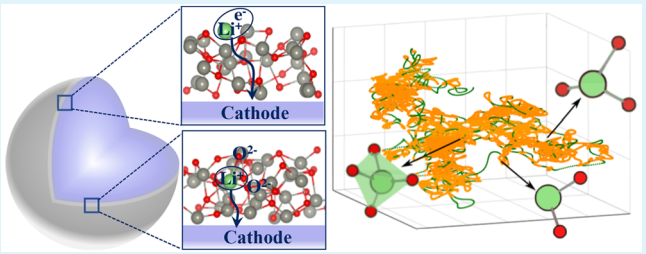

KEYWORDS: *amorphous coating, Li-ion batteries, ion diffusion, ab-initio molecular dynamics, density functional theory calculations*

INTRODUCTION

After dominating the consumer electronics market for several years as rechargeable power sources, lithium-ion batteries (LIBs) are expanding into the automobile industry.[1] However, to sustain continuous growth of electrified transportation, improvements in several areas are needed, including the development of novel stable cathode materials,[2] stable anode materials,[3] new electrolytes,[4] and electrolyte additives that can mitigate side reactions between the electrode materials and the electrolytes.[5] Such side reactions cause a variety of undesirable effects including cation dissolution and associated surface structural degradation, thickening of the solid−electrolyte interphase layer, and large irreversible capacity and coulombic efficiency loss.[6] For example, hydrofluoric acid (HF), formed by degradation of the $LiPF_6$-based electrolyte, is known to attack the cathode particles and accelerate redox-active metal dissolution, thereby lowering the capacity retention upon cycling.[7,8] Others have reported that the rate of detrimental side reactions increases with the state of charge (SOC), temperature, storage time, and cut-off voltage.[9,10] In addition, oxygen loss from high-voltage cathode materials accelerates capacity/voltage fade and jeopardizes the safety of LIBs.[11,12] The oxygen can react with the carbonate electrolyte to yield various carbonate gases and undermine cycling stability.[13] Therefore, enhanced stabilization of the electrode surface is desirable to achieve a highly stable and safe performance of the LIBs.

A common approach to suppress cathode degradation and slow down the cathode−electrolyte side reactions is to apply a protective coating on the cathode surface. Because of the demonstration of improved capacity retention in Al_2O_3-coated $LiCoO_2$,[14] numerous studies on Al_2O_3 and many other coating materials, such as phosphates, carbonates, fluorides, and oxides, have been reported to improve capacity, capacity retention, and rate capability of the cathodes.[15] The underlying mechanisms proposed to explain the improved performance of coated cathode materials include: (1) improved charge

Received: June 1, 2020
Accepted: July 13, 2020
Published: July 13, 2020

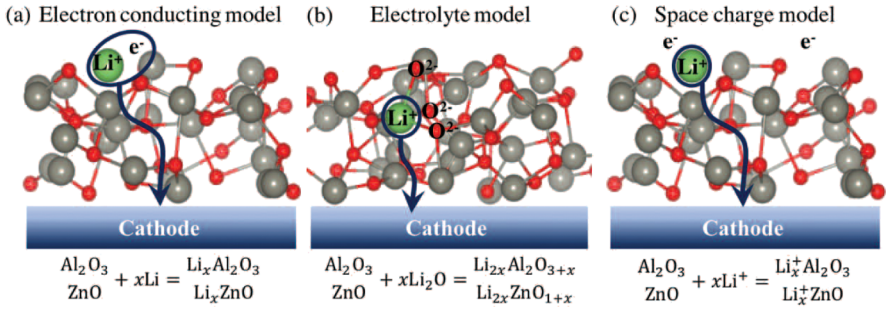

Figure 1. Schematic illustrations of Li^+ transport models in amorphous coatings. (a) Electron-conducting model, where the Li^+ accompanies the electron through a sufficiently electronically conductive coating. (b) Electrolyte model, where the electronically insulating coating acts as an electrolyte that incorporates Li^+ with compensating negative charge in the coating. (c) Space charge model, where Li^+ tunnels through an electronically insulating coating without an accompanying electron.

transfer at the cathode surface; (2) modification of the cathode surface chemistry; (3) decreased reaction with HF in the electrolyte; and (4) formation of a physical barrier between the cathode and electrolyte.[16] Despite the significant body of work focusing on coated cathode materials, developing an optimal coating and understanding the many possible roles of coating materials for specific cathode materials is still challenging as a coating material may enhance one aspect of performance while hindering another. For example, both Al_2O_3 and ZnO coatings have been reported to improve the structural and electrochemical properties of cathode materials;[17,18] however, because of their insulating character, the film thickness should be properly tuned to avoid the coating layer from reducing the capacity and rate behavior.[19,20] Furthermore, most reports focus on the lithium transport in various coating materials, however, the oxygen transport should be considered as well, as oxygen loss is responsible for increased surface impedance, capacity fade, and thermal runaway, especially for high-voltage cathodes.[21] Therefore, besides the aforementioned four functionalities, an optimal coating material should also retain oxygen and hence improve the thermal stability of the cathodes.[20,22,23]

In this work, we present a framework for calculating and analyzing Li^+ and O^{2-} transport as well as the electrochemical stability in cathode-coating materials. Specifically, we target amorphous coating materials, as amorphous films tend to be more conformal, with reduced grain boundaries, dislocations, or other highly defective regions that exist in polycrystalline films. Therefore, amorphous coatings are more likely to reduce the kinetics of O^{2-} transport and effectively suppress corrosion.[24] Furthermore, most coatings exhibit amorphous character,[17,18] although coatings with polycrystalline domains can be achieved depending on the synthesis methods and conditions.[25,26] Our framework includes systematic workflows of *ab-initio* molecular dynamics (AIMD) calculations to obtain representative amorphous structures and associated diffusion trajectories coupled with an analysis of critical changes in the local environment of the active ion during diffusion. Based on these data, we provide an estimate of room-temperature diffusivities, including statistical error bars, and the evaluation of material's suitability in terms of its ability to facilitate Li^+ transport while blocking O^{2-} transport. Finally, we add an analysis of thermodynamic stability of the coating chemistry as a function of the cathode SOC. We implement this framework to study two commonly used amorphous coating materials, Al_2O_3 and ZnO, and make recommendations based on the analyses.

COMPUTATIONAL DETAILS AND STRUCTURAL MODELING

Density functional theory (DFT) electronic structure calculations were performed using the Vienna *Ab-initio* Simulation Package,[27,28] with projector augmented wave potentials.[29] The generalized gradient approximation as parameterized by Perdew–Burke–Ernzerhof (PBE)[30] was used for the exchange–correlation functional. Because of the large unit cells describing the amorphous state, we employed Γ-point-only Brillouin zone integration at a plane-wave cutoff energy of 400 eV and a time step of 2 fs in the AIMD simulations.

For optimal relevance to industrially relevant materials, we focused on conformal ultrathin coatings,[18,31] where defect chemistry and impurity content could lead to off-stoichiometry and some electronic conductivity.[32−34] Hence, the exact composition may be ambiguous and motivates us to employ more generalized models for capturing the range of possible electronic and ionic transport through the thin amorphous layer. Recently, Xu *et al.*[35] have clearly formulated three different scenarios of Li^+ diffusion in thin coatings (see Figure 1): (1) the electron conducting model, where the Li^+ accompanies the electron through a sufficiently electronically conductive coating, which requires that the coating cation(s) are reduced during Li^+ diffusion; (2) the electrolyte model, where the electronically insulating coating acts as an electrolyte that incorporates Li^+ with compensating negative charge in the coating. In this model, the inherent coating cation charge is not affected; (3) the space charge model, where Li^+ tunnels through an electronically insulating coating without an accompanying electron, however, at the cost of a space charge build-up because of the absence of negative compensating charge. The space charge model was ruled out as the build-up electric field exceeds the dielectric breakdown strength for reasonable coating thicknesses (>1 nm) and disagrees with observed overpotential behavior.[35]

In this work, we focus on understanding transport and stability in two known coating materials, Al_2O_3 and ZnO, and employ both the electron conduction model (1) as well as the electrolyte model (2), as illustrated in Figure 1a,b. To simulate the electron-conducting model, we inserted extra Li^0 into amorphous Al_2O_3 and ZnO to generate $Li_{2x}Al_2O_3$ and $Li_{2x}ZnO$, respectively, with Al^{3+} and Zn^{2+} being consequently reduced.[36] This model is similar to previous studies on lithiated amorphous Al_2O_3.[36,37] However, a very high degree of lithiation of Al_2O_3 was employed, up to $Li_{3.4}Al_2O_3$, such that a majority of the coating cation Al^{3+} are reduced to Al^{2+} and Al^+. It is worth noting that Al^{2+} and Al^+ are not stable and

https://dx.doi.org/10.1021/acsami.0c10000
ACS Appl. Mater. Interfaces XXXX, XXX, XXX−XXX

commonly only exist in the gas phase;[38] hence, we expect that only a finite amount of Li^+ and accompanying electrons may be absorbed by Al_2O_3. For this reason, we considered a maximum of 1.1 ($Li^+ + e^-$) per Al_2O_3 unit, that is, $Li_{1.1}Al_2O_3$. The electron-conducting model may be physically motivated by the propensity for high-dielectric constant oxides such as Al_2O_3 to form oxygen vacancies[39,40] and ZnO as a well-known n-type semiconductor.[41] To simulate the electrolyte model, we inserted noncharged Li_2O, representing the "solvated" Li^+ cation into amorphous Al_2O_3 and ZnO to generate $Li_{2x}Al_2O_{3+x}$ and $Li_{2x}ZnO_{1+x}$, respectively. In this model, similar to the diffusion of Li^+ cations in an electrolyte, there are two transport mechanisms for Li^+ diffusion: (1) vehicular diffusion, where the Li^+ diffuses with its coordination shell and (2) structural diffusion, where the Li^+ moves by bond-breaking/formation and exchanging O^{2-} anions in its solvating shell. These two diffusion mechanisms can also be applied to O^{2-} diffusion.

We implemented a "liquid-quench" process to generate the amorphous structures, in which heating, equilibration, and quenching were done through an AIMD workflow, which has been used previously for simulations of Si/SiO_2 lithiation behavior[42] as well as understanding the structure of self-passivating layers.[24] The initial amorphous structures were generated by Packmol package[43] consisting of 100 atoms of Al_2O_3 or ZnO with extra xLi_2O ($2xLi$) for electrolyte (electron conducting) models. For the Al_2O_3 thin film grown by atomic layer deposition (ALD), the O/Al atomic ratio is typically higher than 1.5.[44] On the other hand, there are excess Zn^{2+} ions in the ZnO film by ALD, with $O/Zn < 1$.[45] To generate the liquid phases of the amorphous structures, the initial structures were "heated" at 3000 K, and a sequence of 4 ps AIMD simulations in the *NVT* ensemble were employed to equilibrate the external pressure, wherein the cell volume is rescaled according to the average external pressure before the next AIMD simulation until the averaged external pressure was below 5 kbar in a 2 ps duration. Another approach to equilibrate the external pressure and find the optimal volume is sampling several AIMD simulations with different lattice constant scale factors, thus obtaining the lowest energy state.[46] The energy equilibration was achieved when the difference between the averaged energy per atom in a 2 ps duration and the averaged energy per atom in a 4 ps duration is smaller than 1 meV/atom. Next, the liquid phases were simulated for additional 10 ps, from which three independent configurations were selected and quenched to 0 K to obtain the ground-state atomic positions in the amorphous structures. The quenching workflow consists of a sequence of 0.4 ps AIMD simulations, with the temperature being reduced by 500 K at each quench step. To ensure a slow quench process, we also equilibrated the structure for additional 1 ps after each quench step. The radial distribution functions (RDFs) of Al−O and Zn−O pairs in all the electrolyte and electron-conducting models at 0 K are plotted in Figure S1a−d. Comparing to previous work on amorphous Al_2O_3 and ZnO,[36,47] the RDFs for the generated structures in this work show similar bond lengths and coordination environments. The Al−O and Zn−O bond lengths remain unchanged with an increase of Li^+ content and are estimated to be 1.8 and 2.0 Å, respectively. The O coordination numbers for Al and Zn in electrolyte models stay relatively unchanged while decreasing almost linearly in electron-conducting models (see Figure S1e,f). To perform the diffusion analysis, a series of ionic diffusion trajectories at T = 1400, 1600, 1800, 1900, 2000, 2100, and 2200 K were generated according to the following procedure: for each configuration, we equilibrated the structure at different temperatures and then simulated an 80 ps diffusion trajectory at the corresponding temperature. In the end, there were three diffusion trajectories for each temperature. Figure S2 in the Supporting Information illustrates the entire AIMD and DFT workflows, which were built on the pymatgen,[48] custodian,[48] fireworks,[49] and atomate[50] codes and can be found as part of the open-source mpmorph package at http://github.com/materialsproject/mpmorph.

As part of our analyses, we extract features within ionic diffusion trajectories, such as vibrational motion at fixed sites and translational motion between two sites.[37,46,51] Specifically, ions localized at a particular site for several oscillation periods are deemed vibrational motion while hopping to another site represents translational motion. To capture the ionic vibrational and translational motions, we apply density-based spatial clustering of applications with noise on each obtained diffusion trajectory. For these separate motions, we characterize the changes in local coordination environments during the ionic diffusion by calculating the number of nearest neighbors.

The self-diffusion coefficients (D) of Li^+ and O^{2-} ions in amorphous Al_2O_3 and ZnO were obtained using the Einstein relation: $D = d\langle \delta r^2 \rangle / 6dt$, where t represents timestep, r represents the ion position, and $\langle \delta r^2 \rangle$ represents the mean square displacement (MSD). As the linear MSD *versus* t relation does not hold for all the ranges of timesteps,[52] we exclude the ballistic region at short t and the poor statistical region at large t when linearly fitting D. We calculate the MSD of each ion within temperature window of 1400−2200 K and determine the corresponding D values. Figure S3 illustrates the MSD of Li^+ and O^{2-} ions in amorphous $Li_{0.3}Al_2O_3$, $Li_{0.3}Al_2O_{3.15}$, $Li_{0.12}ZnO$, and $Li_{0.12}ZnO_{1.06}$ at various temperatures. It should be pointed out that the D value at each temperature was averaged over three independent diffusion trajectories (as mentioned earlier). As ionic diffusion in slow diffusers at room temperature is not accessible from direct AIMD simulations because of the low rate of ion hops, the D values at room temperature were extrapolated from those at high temperatures using the Arrhenius relation of D as a function of T: $D = D_0 \exp(-E_a/k_B T)$, where k_B is the Boltzmann constant, D_0 is the pre-exponential factor, and E_a is the activation energy of ion diffusion, which can be determined by fitting the data of $\log D$ *versus* $1/T$ to the Arrhenius relation. Moreover, compared to the diffusion trajectories at higher temperatures, the trajectories at lower temperatures typically exhibit fewer ion hops, thus yielding fitted D values with higher statistical uncertainty.[52] Therefore, we take into account the statistical uncertainty of the D value at each temperature when fitting the Arrhenius relation by assigning the standard deviation of $\log D$ as the weight for each averaged D. Figures S4 and S5 in the Supporting Information display the Arrhenius plots for all the amorphous compounds considered in this work.

RESULTS AND DISCUSSION

To obtain an understanding of the transport mechanisms, we investigate how Li^+ and O^{2-} diffuse through the amorphous coating and the chemical coordination environments that enhance or limit their diffusion. For illustration of representative trends, we plot the trajectories of one Li^+ and one O^{2-} in $Li_{0.3}Al_2O_{3.15}$ (Figure 2a,b) and $Li_{0.12}ZnO_{1.06}$ (Figure

https://dx.doi.org/10.1021/acsami.0c10000
ACS Appl. Mater. Interfaces XXXX, XXX, XXX−XXX

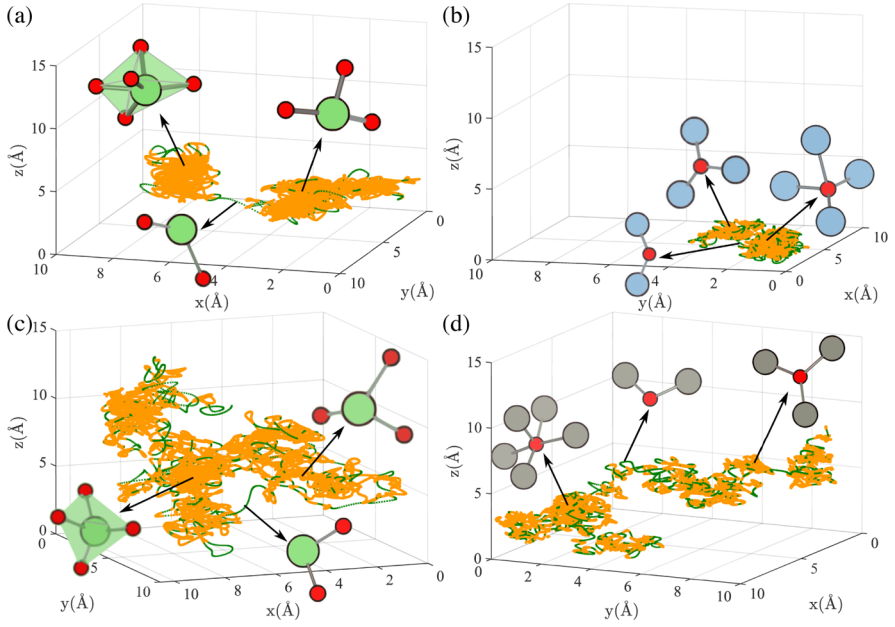

Figure 2. Trajectories of one Li^+ and one O^{2-} in amorphous $Li_{0.3}Al_2O_{3.15}$ (a,b) and $Li_{0.12}ZnO_{1.06}$ (c,d) at 2000 K for 40 ps. Yellow and green dots represent vibrational and translational motions, respectively.

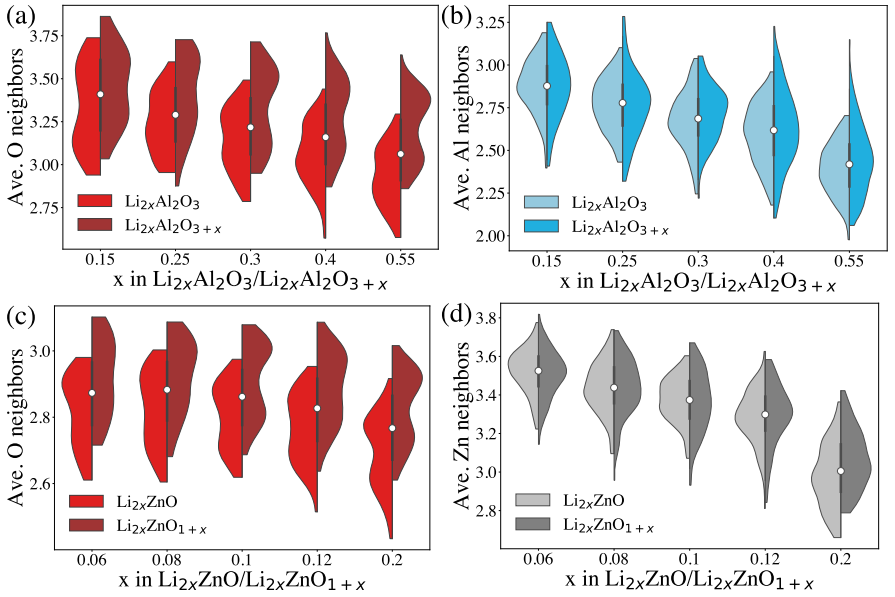

Figure 3. Averaged number of O neighbors during Li^+ diffusion (a,c) and averaged number of Al and Zn neighbors during O^{2-} diffusion (b,d) for amorphous Al_2O_3 and ZnO at 2000 K for 40 ps.

2c,d) at 2000 K for 40 ps. It is evident from the figures that the Li^+ diffuses longer distances than the O^{2-} ion during the same amount of time. Also, both Li^+ and O^{2-} diffuse significantly faster in ZnO than in Al_2O_3. The trajectories of Li^+ and O^{2-} ions, as shown in Figure 2, also show their active vibrational and translational motions, which are represented by the yellow and green dots, respectively, as shown in Figure 2. We observe that the Li^+ and O^{2-} ions vibrate around their local minimum positions and then translate to another local minimum state by passing through the intermediate and activated state. For each time step, we analyze the number of nearest neighbors of the Li^+ and O^{2-} ions during the vibrational and translational motions to elucidate the changes of chemical coordination environments during the ion diffusion. We find that during vibrational motion, Li^+ is bonded to more O^{2-} ions than during translational motions, which implies that Li^+ is trapped at its local equilibrium site by the neighboring O^{2-} ions, and its translation to another vibration site is initiated by the Li−O bond breaking/formation process. Similarly, the O^{2-} ion is trapped by its neighboring cations, that is, Al^{3+}, Zn^{2+}, or Li^+, and its translation is promoted by breaking cation−anion bonds. We note that this analysis is in agreement with previously proposed ionic conduction mechanism in amorphous Al_2O_3, $Na_2Si_2O_5$, and SiO_2.[37,46,53]

To further improve our understanding on diffusion-promoting motifs, we calculate the number of nearest neighbors of Li^+ and O^{2-} ions for electron-conducting and electrolyte models to characterize the changes in local

https://dx.doi.org/10.1021/acsami.0c10000
ACS Appl. Mater. Interfaces XXXX, XXX, XXX−XXX

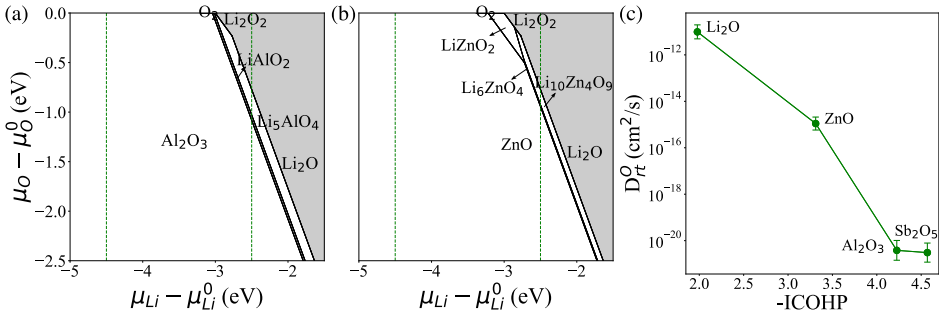

Figure 4. Phase diagram of Li−Al−O (a) and Li−Zn−O (b) systems as a function of Li and O chemical potentials. All the compositions are in amorphous phases. The green dash lines represent a typical high-voltage Li-ion battery operating voltage 2.5−4.5 V *vs* Li metal. (c) Calculated O^{2-} room-temperature self-diffusion coefficients and −ICOHP values for amorphous Li_2O, Al_2O_3, ZnO, and Sb_2O_5.

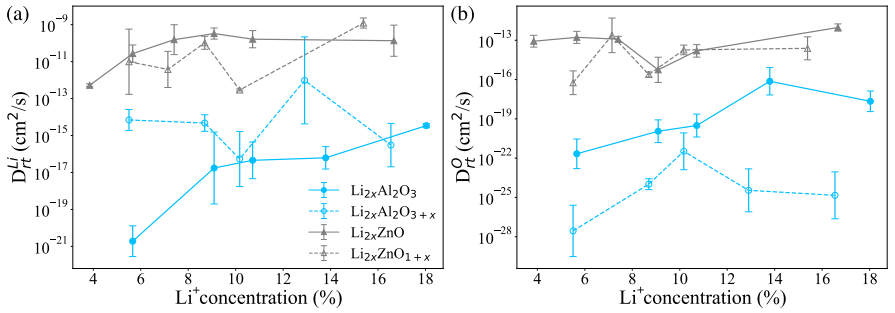

Figure 5. Calculated room-temperature self-diffusion coefficients of Li^+ (a) and O^{2-} (b) in Al_2O_3 and ZnO as a function of Li^+ concentration. Blue and gray lines represent Al_2O_3 and ZnO, respectively. Solid and dashed lines represent electron-conducting and electrolyte models, respectively.

coordination environments as a function of Li^+ concentration during diffusion. In Figure 3, we present the average number of O^{2-} neighbors during Li^+ diffusion and the average number of Al^{3+}/Zn^{2+} neighbors during O^{2-} diffusion for $Li_{2x}Al_2O_3/Li_{2x}Al_2O_{3+x}$ and $Li_{2x}ZnO/Li_{2x}ZnO_{1+x}$ at 2000 K for 40 ps. Consistently, we observe a decrease in the O^{2-} coordination number with Li^+ during Li^+ diffusion and similarly the number of $Al^{3+}(Zn^{2+})$ neighbors during O^{2-} diffusion, as a function of increasing Li^+ concentration. This implies a higher Li^+ as well as O^{2-} mobility in amorphous structures with higher Li^+ content. In addition, the number of O^{2-} neighbors during Li^+ diffusion in ZnO is smaller than that in Al_2O_3, consistent with a higher Li^+ diffusivity in ZnO. On the other hand, in ZnO, the O^{2-} ion exhibits a higher coordination number to Zn^{2+} neighbors as compared to Al^{3+} in Al_2O_3. However, as shown below, the Al−O bond is stronger than the Zn−O bond such that the bond-breaking process necessary for translation is less favorable in Al_2O_3 as compared to ZnO. Therefore, the O^{2-} diffusivity is limited by both the cation coordination number and the cation−oxygen bond strength.

The trends toward higher ionic diffusivity (both Li^+ and O^{2-}) with higher Li^+ content of the coating beg the question if such Li-containing coatings are thermodynamically stable at high charge. To estimate the stability of Li-containing coating materials, we calculate the phase diagram of the amorphous Li−Al−O and Li−Zn−O systems as a function of Li and O chemical potentials, as shown in Figure 4a,b. We emphasize that all phases were generated from the compounds in their amorphous structures, which were obtained from the "liquid-quench" process outlined in previous section. In Figure S6, we also plot the phase diagrams of Li−Al−O and Li−Zn−O systems using the crystalline phases. Recently, Aykol *et al.* have proposed a thermodynamic upper limit on the energy scale for synthesizability of metastable crystalline polymorphs.[54] At 0 K, the energy limit is defined on the basis of the amorphous state, above which a polymorph cannot be stabilized. Therefore, the Gibbs free energy of amorphous phase is higher than that of its synthesizable polymorph counterparts. For Al_2O_3, ZnO, and Li_2O, the amorphous limits are all approximately 0.2 eV/atom.[54] The vertical green dash lines, as shown in Figure 4, represent a typical operating voltage of 2.5−4.5 V *versus* Li metal for high-voltage cathode materials. We observe several Li-containing phases to be synthetically accessible. One example is Li_6ZnO_4, which indeed has been experimentally confirmed in ZnO-coated cathodes.[55] However, at a high charge state, Li-containing Al oxide or Zn oxide phase, such as $LiAlO_2$ and Li_6ZnO_4, are unstable and are expected to delithiate and decompose to Al_2O_3 and ZnO, respectively. This conclusion is in good agreement with the experimental results, where the Al_2O_3 surface film is stable against electrochemical charge and discharge between 2.0 and 4.6 V, and no Li-containing Al oxide has been detected.[17] On the other hand, it should be noted that the surface Al_2O_3 layer can be lithiated to form a stable Li−Al−O glass, for example, $LiAlO_2$, but at a much lower cycling voltage, for example, 1 mV to 2.5 V.[56,57] These results indicate that while a higher Li^+ content may promote higher ionic diffusion, low Li^+ content of Al_2O_3 and ZnO coating formulations provide a more realistic model given stability constraints from exposure to highly charged cathodes.

Using the methodology described in the previous section, we estimate the room-temperature self-diffusion coefficients of Li^+ (D_{rt}^{Li}) and O^{2-} (D_{rt}^{O}) in Al_2O_3 and ZnO. Figure 5 shows the extrapolated D_{rt}^{Li} and D_{rt}^{O} values as a function of Li^+ concentration. Tables S1 and S2 list the calculated activation energy E_a, pre-exponential factor D_0, extrapolated D_{rt}, and conductivity C_{rt} for Li^+ and O^{2-} diffusion in all the considered compositions. Our calculated E_a of Li^+ diffusion in Al_2O_3 is

https://dx.doi.org/10.1021/acsami.0c10000
ACS Appl. Mater. Interfaces XXXX, XXX, XXX−XXX

close to the experimental values reported by Glass and Nassau in $Li_2O-Al_2O_3$ glasses.[58] Three observations regarding the variance of D_{rt} values can be extracted: (1) in general, a higher Li^+ content leads to higher D_{rt}^{Li} and D_{rt}^{O} values, which corresponds well with the decreased O^{2-} coordination number of Li^+ as well as the lower cation (Al^{3+}/Zn^{2+}) coordination number of O^{2-} during diffusion (*e.g.*, translational motion), as shown in Figure 3. (2) Compared with the electron-conducting model, the electrolyte model results in faster Li^+ diffusion in Al_2O_3. This suggests that the significantly impeded electron hopping[59] in amorphous Al_2O_3 would present a bottleneck for Li^+ transport. Interestingly, there is no major difference in D_{rt}^{Li} between the electron-conducting and the electrolyte models in ZnO, which implies that the electron mobility in semiconducting ZnO is fast enough to support Li^+ diffusion. Indeed, the room-temperature electrical conductivity of ZnO is orders of magnitude higher than that of Al_2O_3.[60,61] Furthermore, the electron-conducting model promotes O^{2-} transport in Al_2O_3, which suggests that the reduced Al cations exhibit a weaker bond to oxygen, while Al cations remain 3+ state in the electrolyte model. (3) We find that Li^+ and O^{2-} diffuse significantly faster in ZnO than in Al_2O_3. For Li^+ diffusion, this is mainly rationalized by the lower oxygen coordination number for Li^+ in ZnO, as compared to that of Al_2O_3 (Figure 3a,c). However, to analyze the factors affecting O^{2-} diffusion, we estimate the variance of bond strength between Al−O and Zn−O. To obtain a quantitative measure of the bond strength, we calculate the averaged integration of projected crystal orbital Hamiltonian populations (ICOHP) up to the Fermi level of Al−O and Zn−O in amorphous Al_2O_3 and ZnO, respectively, using the LOBSTER codes.[62] The averaged ICOHP values are determined by averaging over all the ICOHP values of metal−O bonds that exhibit a bond length less than 2.6 Å. The results are shown in Figure 4c along with the D_{rt}^{O} and ICOHP values of amorphous Li_2O and Sb_2O_5 for comparison. It can be seen that a higher −ICOHP value of metal−O bond corresponds to a lower D_{rt}^{O}, and the −ICOHP value of Al−O bond (4.13 eV) is higher than that of Zn−O bond (3.31 eV), which suggests a stronger Al−O bond as compared to Zn−O. Therefore, the slower diffusion of O^{2-} in Al_2O_3 with its underlying cation-oxygen bond-breaking mechanism can be rationalized by the stronger Al−O bond as compared to the Zn−O one, even though amorphous ZnO exhibits a higher cation-oxygen coordination number than amorphous Al_2O_3.

Finally, using the obtained transport results, we estimate and discuss the impact of coating material choice on a model cathode performance, addressing facile Li^+ transport while attempting to impede O^{2-} transport. Assuming a spherical $LiNiO_2$ model cathode particle of 10 μm in diameter[63] and a Li^+ diffusivity of $D_{rt}^{Li} = 10^{-10}$ cm^2/s in $LiNiO_2$,[2] produces an averaged time of 625 s for Li^+ to transport from the inner particle to the surface. A lower bound coating thickness of 1 nm and an estimated Li^+ diffusivity in Al_2O_3 of $D_{rt}^{Li} = 10^{-16}$ cm^2/s result in a Li^+ transport time of 100 s through the coating, which is 14% of the total transport time from the cathode particle into the electrolyte. However, a thicker coating of 10 nm[64] increases the estimated Li^+ diffusion time within the coating to 10,000 s, increasing the total diffusion time to 10,625 s. Hence, thick conformal Al_2O_3 coatings could significantly reduce Li-ion conductivity and rate capability of the electrode.[19,65] However, it is worth pointing out that an Al_2O_3 coating can substantially reduce the kinetics of oxygen transport from the electrode to the electrolyte because of the low O^{2-} diffusivity in Al_2O_3. For example, considering $D_{rt}^{O} = 10^{-20}$ cm^2/s, even with 1 nm Al_2O_3 conformal coating, the estimated time for O^{2-} to transport through the coating would be 10^6 s. Turning to ZnO, an 1 nm coating and an estimated Li^+ diffusivity of $D_{rt}^{Li} = 10^{-10}$ cm^2/s result in an estimated time of 100 μs for Li^+ transport through the coating. However, the corresponding analysis, assuming $D_{rt}^{O} = 10^{-14}$ cm^2/s, for O^{2-} diffusion yields 1 s, which indicates that amorphous ZnO would not be preferred for high-voltage oxide cathode coatings, despite facile Li^+ diffusion properties. It should be noted that our estimated diffusion time is based on self-diffusion, that is, we neglect the driving force of the chemical potential gradient across the coating. Thus, our estimation is likely a lower bound approximation for the Li^+ and O^{2-} transport; however, the consideration of a chemical potential difference between the cathode and electrolyte will affect each coating equally. Overall, we predict that Al_2O_3 would be a better conformal coating for high-voltage oxide cathodes as compared to ZnO, however, care should be taken to limit the thickness.

Based on the Li^+ and O^{2-} transport behavior in Al_2O_3 and ZnO, we find, not surprisingly, that in these materials, Li^+ transport is correlated with O^{2-} transport, that is, a slower O^{2-} diffusion in Al_2O_3 leads to a slower Li^+ diffusion. However, we stress that such correlation may only hold in binary oxides. For example, in chlorides or bromides, Li^+ is likely to bond to Cl^- or Br^-, interfering less with the transport of any possible neighboring O^{2-} ions. In such materials, Li^+ translation is likely initiated by a Li−Cl or Li−Br bond breaking/formation process. Interestingly, Li_3YCl_6 and Li_3YBr_6 have been found to exhibit high-room temperature Li-ion conductivity as the solid−electrolyte materials.[66] Along with their high chemical and electrochemical stability, Li_3YCl_6 and Li_3YBr_6 also show promise as cathode-coating materials. In addition, numerous polyanionic oxides, such as NASICON- and LISICON-type phosphates,[67,68] have also been proposed to exhibit high-room temperature Li-ion conductivity. The covalency of oxygen with the nonmetal cation in the polyanion also enhances the bond strength with O^{2-} and increases the oxidation limit of polyanionic oxides.[69] Therefore, polyanionic oxides are likely a promising category of cathode-coating materials from the perspective of facile Li^+ transport and impeded O^{2-} transport.

CONCLUSIONS

Today's LIB materials rely on engineering solutions to perform at conditions far from their equilibrium. For example, cathode degradation at high charge is commonly suppressed by applications of physical barriers in the form of thin protective coatings, which are ideally transparent to the active Li^+ ion, while suppressing oxygen release from the cathode as well as undesirable reactions with the electrolyte. These thin, noncrystalline, and defective coating materials and their functionality as a function of chemistry and structure are extremely difficult to characterize and monitor in situ. To improve our understanding and future rational design of optimal cathode coating materials for Li-ion energy storage applications, we here explore transport mechanisms and thermodynamic stability in two known amorphous coating materials: Al_2O_3 and ZnO. We use extensive AIMD to produce reasonable model systems for the amorphous phases and explore the diffusion of Li^+ and O^{2-} as a function of Li^+ content. Given the uncertainty of transport modes in these noncrystalline coatings, we employ two different models to

https://dx.doi.org/10.1021/acsami.0c10000
ACS Appl. Mater. Interfaces XXXX, XXX, XXX−XXX

capture the diffusion behavior: (1) electron-conducting model and (2) electrolyte model. The following observations and conclusions are made:

(1) In general, higher Li^+ content improves both Li^+ and O^{2-} transport in Al_2O_3 and ZnO, which is rationalized by the lower coordinating number of neighboring O^{2-} and Al^{3+} (Zn^{2+}) ions, respectively. Also, Li^+ and O^{2-} diffuse much faster in ZnO than in Al_2O_3. In ZnO, ionic transport is facilitated by the lower oxygen coordinations during Li^+ diffusion, as well as the higher electronic conductivity. In Al_2O_3, the stronger Al−O bond impedes the bond-breaking mechanism necessary for oxygen translational motion.

(2) Considering both Li^+ diffusivity as well as O^{2-} transport as selection metrics, Al_2O_3 provides a better conformal cathode coating than ZnO. However, its coating thickness should be thin (1 nm) to avoid the coating layer from negatively impacting the Li-ion conductivity and capacity of the electrode.

(3) For Al_2O_3 and ZnO, even though their lithiated counterparts, such as $LiAlO_2$, can achieve a faster Li^+ diffusion, they are not stable against delithiation and subsequent decomposition at a state of high charge.

In summary, we present a framework to study amorphous materials as the conformal coating for high-voltage cathodes. The framework includes series of AIMD simulations to obtain amorphous structures and diffusion trajectories, the analysis of the change in coordinating environments during diffusion, the estimation of room temperature diffusivities, and finally, the evaluation of the coating suitability in terms of its ability to facilitate Li^+ transport while blocking O^{2-} transport. We believe this framework can be productively used to study other amorphous metal oxides, such as MgO and Ta_2O_5, and fluorides, such as AlF_3 and CaF_2, and to help design new chemical-coating formulations.

■ ASSOCIATED CONTENT

Supporting Information

The Supporting Information is available free of charge at https://pubs.acs.org/doi/10.1021/acsami.0c10000.

RDFs and oxygen coordination number for $Li_{2x}Al_2O_3$, $Li_{2x}Al_2O_{3+x}$, $Li_{2x}ZnO$, and $Li_{2x}ZnO_{1+x}$; schematic illustration of AIMD and DFT workflows; MSD of Li^+ and O^{2-} ions; Arrhenius plots of Li^+ and O^{2-} self-diffusivity D; O^{2-} self-diffusivity D in amorphous oxides; phase diagram of Li−Al−O and Li−Zn−O systems; and calculated activation energy E_a, pre-exponential factor D_0, extrapolated room-temperature diffusivity D_{rt}, and conductivity C_{rt} (PDF)

■ AUTHOR INFORMATION

Corresponding Author

Kristin A. Persson − *Department of Materials Science and Engineering, University of California, Berkeley, California 94720-1760, United States; Energy Storage and Distributed Resources Division, Lawrence Berkeley National Laboratory, Berkeley, California 94720, United States;* orcid.org/0000-0003-2495-5509; Email: kapersson@lbl.gov

Authors

Jianli Cheng − *Department of Materials Science and Engineering, University of California, Berkeley, California 94720-1760, United States; Energy Storage and Distributed Resources Division, Lawrence Berkeley National Laboratory, Berkeley, California 94720, United States;* orcid.org/0000-0002-0302-7861

Eric Sivonxay − *Department of Materials Science and Engineering, University of California, Berkeley, California 94720-1760, United States; Energy Storage and Distributed Resources Division, Lawrence Berkeley National Laboratory, Berkeley, California 94720, United States*

Complete contact information is available at: https://pubs.acs.org/10.1021/acsami.0c10000

Notes

The authors declare no competing financial interest.

■ ACKNOWLEDGMENTS

The authors thank Dr. Gerbrand Ceder and Kara D. Fong for useful discussions. This work was intellectually led by the Battery Materials Research (BMR) program under the Assistant Secretary for Energy Efficiency and Renewable Energy, Office of Vehicle Technologies of the U.S. Department of Energy, Contract DEAC02-05CH11231. This research used resources of the National Energy Research Scientific Computing Center (NERSC).

■ REFERENCES

(1) Myung, S.-T.; Maglia, F.; Park, K.-J.; Yoon, C. S.; Lamp, P.; Kim, S.-J.; Sun, Y.-K. Nickel-Rich Layered Cathode Materials for Automotive Lithium-Ion Batteries: Achievements and Perspectives. *ACS Energy Lett.* **2017**, *2*, 196−223.

(2) Ryu, H.-H.; Park, G.-T.; Yoon, C. S.; Sun, Y.-K. Suppressing Detrimental Phase Transitions via Tungsten Doping of LiNiO2 Cathode for Next-generation Lithium-ion Batteries. *J. Mater. Chem. A* **2019**, *7*, 18580−18588.

(3) Wang, H.; Fu, J.; Wang, C.; Wang, J.; Yang, A.; Li, C.; Sun, Q.; Cui, Y.; Li, H. A binder-free high silicon content flexible anode for Li-ion batteries. *Energy Environ. Sci.* **2020**, *13*, 848−858.

(4) Cao, X.; Xu, Y.; Zhang, L.; Engelhard, M. H.; Zhong, L.; Ren, X.; Jia, H.; Liu, B.; Niu, C.; Matthews, B. E.; Wu, H.; Arey, B. W.; Wang, C.; Zhang, J.-G.; Xu, W. Nonflammable Electrolytes for Lithium Ion Batteries Enabled by Ultraconformal Passivation Interphases. *ACS Energy Lett.* **2019**, *4*, 2529−2534.

(5) Li, Y.; Wan, S.; Veith, G. M.; Unocic, R. R.; Paranthaman, M. P.; Dai, S.; Sun, X.-G. A Novel Electrolyte Salt Additive for Lithium-Ion Batteries with Voltages Greater than 4.7 V. *Adv. Energy Mater.* **2017**, *7*, 1601397.

(6) Hu, M.; Pang, X.; Zhou, Z. Review Recent Progress in High-Voltage Lithium Ion Batteries. *J. Power Sources* **2013**, *237*, 229−242.

(7) Edström, K.; Gustafsson, T.; Thomas, J. O. The Cathode-electrolyte Interface in the Li-Ion Battery. *Electrochim. Acta* **2004**, *50*, 397−403.

(8) Jang, D. H.; Oh, S. M. Electrolyte Effects on Spinel Dissolution and Cathodic Capacity Losses in 4 V Li/LixMn2O4 Rechargeable Cells. *J. Electrochem. Soc.* **1997**, *144*, 3342−3348.

(9) Pieczonka, N. P. W.; Liu, Z.; Lu, P.; Olson, K. L.; Moote, J.; Powell, B. R.; Kim, J.-H. Understanding Transition-Metal Dissolution Behavior in LiNi0.5Mn1.5O4 High-Voltage Spinel for Lithium Ion Batteries. *J. Phys. Chem. C* **2013**, *117*, 15947−15957.

(10) Yang, L.; Ravdel, B.; Lucht, B. L. Electrolyte Reactions with the Surface of High Voltage LiNi0.5Mn1.5O4 Cathodes for Lithium-Ion Batteries. *Electrochem. Solid-State Lett.* **2010**, *13*, A95−A97.

(11) Noh, H.-J.; Youn, S.; Yoon, C. S.; Sun, Y.-K. Comparison of the Structural and Electrochemical Properties of Layered Li[NixCoyMnz] O2 (x = 1/3, 0.5, 0.6, 0.7, 0.8 and 0.85) Cathode Material for Lithium-Ion Batteries. *J. Power Sources* **2013**, *233*, 121−130.

(12) Sharifi-Asl, S.; Lu, J.; Amine, K.; Shahbazian-Yassar, R. Oxygen Release Degradation in Li-Ion Battery Cathode Materials: Mechanisms and Mitigating Approaches. *Adv. Energy Mater.* **2019**, *9*, 1900551.
(13) Jung, R.; Metzger, M.; Maglia, F.; Stinner, C.; Gasteiger, H. A. Oxygen Release and Its Effect on the Cycling Stability of LiNixMnyCozO2(NMC) Cathode Materials for Li-Ion Batteries. *J. Electrochem. Soc.* **2017**, *164*, A1361−A1377.
(14) Cho, J.; Kim, Y. J.; Park, B. Novel LiCoO2Cathode Material with Al2O3Coating for a Li Ion Cell. *Chem. Mater.* **2000**, *12*, 3788−3791.
(15) Zuo, D.; Tian, G.; Li, X.; Chen, D.; Shu, K. Recent Progress in Surface Coating of Cathode Materials for Lithium Ion Secondary Batteries. *J. Alloys Compd.* **2017**, *706*, 24−40.
(16) Chen, Z.; Qin, Y.; Amine, K.; Sun, Y.-K. Role of Surface Coating on Cathode Materials for Lithium-Ion Batteries. *J. Mater. Chem.* **2010**, *20*, 7606−7612.
(17) Zhang, X.; Belharouak, I.; Li, L.; Lei, Y.; Elam, J. W.; Nie, A.; Chen, X.; Yassar, R. S.; Axelbaum, R. L. Structural and Electrochemical Study of Al2O3and TiO2Coated Li1.2Ni0.13Mn0.54-Co0.13O2Cathode Material Using ALD. *Adv. Energy Mater.* **2013**, *3*, 1299−1307.
(18) Zhao, J.; Wang, Y. Ultrathin Surface Coatings for Improved Electrochemical Performance of Lithium Ion Battery Electrodes at Elevated Temperature. *J. Phys. Chem. C* **2012**, *116*, 11867−11876.
(19) Jung, Y. S.; Cavanagh, A. S.; Dillon, A. C.; Groner, M. D.; George, S. M.; Lee, S.-H. Enhanced Stability of LiCoO2 Cathodes in Lithium-Ion Batteries Using Surface Modification by Atomic Layer Deposition. *J. Electrochem. Soc.* **2010**, *157*, A75−A81.
(20) Chang, W.; Choi, J.-W.; Im, J.-C.; Lee, J. K. Effects of ZnO Coating on Electrochemical Performance and Thermal Stability of LiCoO2 as Cathode Material for Lithium-Ion Batteries. *J. Power Sources* **2010**, *195*, 320−326.
(21) Wang, Q.; Ping, P.; Zhao, X.; Chu, G.; Sun, J.; Chen, C. Thermal Runaway Caused Fire and Explosion of Lithium Ion Battery. *J. Power Sources* **2012**, *208*, 210−224.
(22) Kweon, H.-J.; Park, J.; Seo, J.; Kim, G.; Jung, B.; Lim, H. S. Effects of Metal Oxide Coatings on the Thermal Stability and Electrical Performance of LiCoCO2 in a Li-Ion Cell. *J. Power Sources* **2004**, *126*, 156−162.
(23) Zhang, Z. R.; Li, J.; Yang, Y. The effects of decomposition products of electrolytes on the thermal stability of bare and TiO2-coated delithiated Li1−xNi0.8Co0.2O2 cathode materials. *Electrochim. Acta* **2006**, *52*, 1442−1450.
(24) Aykol, M.; Persson, K. A. Oxidation Protection with Amorphous Surface Oxides: Thermodynamic Insights from Ab Initio Simulations on Aluminum. *ACS Appl. Mater. Interfaces* **2018**, *10*, 3039−3045.
(25) Zhao, J.; Qu, G.; Flake, J. C.; Wang, Y. Low Temperature Preparation of Crystalline ZrO2 Coatings for Improved Elevated-Temperature Performances of Li-Ion Battery Cathodes. *Chem. Commun.* **2012**, *48*, 8108−8110.
(26) Chen, Z.; Dahn, J. R. Effect of a ZrO2 Coating on the Structure and Electrochemistry of LixCoO2 When Cycled to 4.5 V. *Electrochem. Solid-State Lett.* **2002**, *5*, A213−A216.
(27) Kresse, G.; Furthmüller, J. Efficiency of Ab-Initio Total Energy Calculations for Metals and Semiconductors Using a Plane-Wave Basis Set. *Comput. Mater. Sci.* **1996**, *6*, 15−50.
(28) Kresse, G.; Furthmüller, J. Efficient Iterative Schemes for Ab Initio Total-Energy Calculations Using a Plane-Wave Basis Set. *Phys. Rev. B* **1996**, *54*, 11169−11186.
(29) Kresse, G.; Joubert, D. From Ultrasoft Pseudopotentials to the Projector Augmented-Wave Method. *Phys. Rev. B* **1999**, *59*, 1758−1775.
(30) Perdew, J. P.; Burke, K.; Ernzerhof, M. Generalized Gradient Approximation Made Simple. *Phys. Rev. Lett.* **1996**, *77*, 3865−3868.
(31) Jung, Y. S.; Cavanagh, A. S.; Riley, L. A.; Kang, S.-H.; Dillon, A. C.; Groner, M. D.; George, S. M.; Lee, S.-H. Ultrathin Direct Atomic Layer Deposition on Composite Electrodes for Highly Durable and Safe Li-Ion Batteries. *Adv. Mater.* **2010**, *22*, 2172−2176.
(32) Kim, M.; Kang, K.-M.; Wang, Y.; Park, H.-H. N-doped Al2O3 thin films deposited by atomic layer deposition. *Thin Solid Films* **2018**, *660*, 657−662.
(33) Groner, M. D.; Fabreguette, F. H.; Elam, J. W.; George, S. M. Low-Temperature Al2O3Atomic Layer Deposition. *Chem. Mater.* **2004**, *16*, 639−645.
(34) Li, Y.; Pei, Y.; Hu, R.; Chen, Z.; Ni, Y.; Lin, J.; Chen, Y.; Zhang, X.; Shen, Z.; Liang, J.; Fan, B.; Wang, G.; Duan, H. Charge Trapping Memory Characteristics of Amorphous-Indium-Gallium-Zinc Oxide Thin-Film Transistors With Defect-Engineered Alumina Dielectric. *IEEE Trans. Electron Devices* **2015**, *62*, 1184−1188.
(35) Xu, S.; Jacobs, R. M.; Nguyen, H. M.; Hao, S.; Mahanthappa, M.; Wolverton, C.; Morgan, D. Lithium Transport Through Lithium-Ion Battery Cathode Coatings. *J. Mater. Chem. A* **2015**, *3*, 17248−17272.
(36) Jung, S. C.; Han, Y.-K. How Do Li Atoms Pass through the Al2O3 Coating Layer during Lithiation in Li-ion Batteries? *J. Phys. Chem. Lett.* **2013**, *4*, 2681−2685.
(37) Jung, S. C.; Kim, H.-J.; Choi, J. W.; Han, Y.-K. Sodium Ion Diffusion in Al2O3: A Distinct Perspective Compared with Lithium Ion Diffusion. *Nano Lett.* **2014**, *14*, 6559−6563.
(38) Dohmeier, C.; Loos, D.; Schnöckel, H. Aluminum(I) and Gallium(I) Compounds: Syntheses, Structures, and Reactions. *Angew. Chem., Int. Ed.* **1996**, *35*, 129−149.
(39) Robertson, J. High Dielectric Constant Gate Oxides for Metal Oxide Si Transistors. *Rep. Prog. Phys.* **2006**, *69*, 327−396.
(40) Cartier, E.; Linder, B. P.; Narayanan, V.; Paruchuri, V. K. Fundamental Understanding and Optimization of PBTI in nFETs with SiO 2/HfO2 Gate Stack. *Technical Digest—International Electron Devices Meeting, IEDM*, 2006.
(41) McCluskey, M. D.; Jokela, S. J. Defects in ZnO. *J. Appl. Phys.* **2009**, *106*, 071101.
(42) Sivonxay, E.; Aykol, M.; Persson, K. A. The Lithiation Process and Li Diffusion Inamorphous SiO2 and Si from First-Principles. *Electrochim. Acta* **2020**, *331*, 135344.
(43) Martínez, L.; Andrade, R.; Birgin, E. G.; Martínez, J. M. PACKMOL: A Package Forbuilding Initial Configurations for Molecular Dynamics Simulations. *J. Comput. Chem.* **2009**, *30*, 2157−2164.
(44) Iatsunskyi, I.; Kempiński, M.; Jancelewicz, M.; Załęski, K.; Jurga, S.; Smyntyna, V. Structural and XPS Characterization of ALD Al2O3 Coated Porous Silicon. *Vacuum* **2015**, *113*, 52−58.
(45) Keun Kim, S.; Seong Hwang, C.; Ko Park, S.-H.; Jin Yun, S. Comparison between ZnO Films Grown by Atomic Layer Deposition Using H2O or O3 as Oxidant. *Thin Solid Films* **2005**, *478*, 103−108.
(46) Lei, X.; Jee, Y.; Huang, K. Amorphous Na2Si2O5 as a Fast Na+ Conductor: an Ab Initio Molecular Dynamics Simulation. *J. Mater. Chem. A* **2015**, *3*, 19920−19927.
(47) Roy, A.; Cheng, Y.-T.; Falk, M. L. Amorphous ZnO-Based Compounds as Thermoelectrics. *J. Phys. Chem. C* **2016**, *120*, 2529−2535.
(48) Ong, S. P.; Richards, W. D.; Jain, A.; Hautier, G.; Kocher, M.; Cholia, S.; Gunter, D.; Chevrier, V. L.; Persson, K. A.; Ceder, G. Python Materials Genomics (pymatgen): A Robust, Open-Source Python Library for Materials Analysis. *Comput. Mater. Sci.* **2013**, *68*, 314−319.
(49) Jain, A.; Ong, S. P.; Chen, W.; Medasani, B.; Qu, X.; Kocher, M.; Brafman, M.; Petretto, G.; Rignanese, G.-M.; Hautier, G.; Gunter, D.; Persson, K. A. FireWorks: a Dynamic Workflow System Designed for High-Throughput Applications. *Concurrency Computat.: Pract. Exper.* **2015**, *27*, 5037−5059.
(50) Mathew, K.; Montoya, J. H.; Faghaninia, A.; Dwarakanath, S.; Aykol, M.; Tang, H.; Chu, I.-h.; Smidt, T.; Bocklund, B.; Horton, M.; Dagdelen, J.; Wood, B.; Liu, Z.-K.; Neaton, J.; Ong, S. P.; Persson, K.; Jain, A. Atomate: A High-Level Interface to Generate, Execute, and Analyzecomputational Materials Science Workflows. *Comput. Mater. Sci.* **2017**, *139*, 140−152.

https://dx.doi.org/10.1021/acsami.0c10000
ACS Appl. Mater. Interfaces XXXX, XXX, XXX−XXX

(51) Smith, W.; Greaves, G. N.; Gillan, M. J. Computer Simulation of Sodium Disilicate Glass. *J. Chem. Phys.* **1995**, *103*, 3091−3097.
(52) He, X.; Zhu, Y.; Epstein, A.; Mo, Y. Statistical Variances of Diffusional Properties from Ab Initio Molecular Dynamics Simulations. *npj Comput. Mater.* **2018**, *4*, 18.
(53) Ostadhossein, A.; Kim, S.-Y.; Cubuk, E. D.; Qi, Y.; van Duin, A. C. T. Atomic Insight into the Lithium Storage and Diffusion Mechanism of SiO2/Al2O3 Electrodes of Lithium Ion Batteries: ReaxFF Reactive Force Field Modeling. *J. Phys. Chem. A* **2016**, *120*, 2114−2127.
(54) Aykol, M.; Dwaraknath, S. S.; Sun, W.; Persson, K. A. Thermodynamic Limit for Synthesis of Metastable Inorganic Materials. *Sci. Adv.* **2018**, *4*, No. eaaq0148.
(55) Fang, T.; Duh, J.-G.; Sheen, S.-R. Improving the Electrochemical Performance of LiCoO2 Cathode by Nanocrystalline ZnO Coating. *J. Electrochem. Soc.* **2005**, *152*, A1701−A1706.
(56) Xiao, X.; Lu, P.; Ahn, D. Ultrathin Multifunctional Oxide Coatings for Lithium Ion Batteries. *Adv. Mater.* **2011**, *23*, 3911−3915.
(57) Liu, Y.; Hudak, N. S.; Huber, D. L.; Limmer, S. J.; Sullivan, J. P.; Huang, J. Y. In Situ Transmission Electron Microscopy Observation of Pulverization of Aluminum Nanowires and Evolution of the Thin Surface Al2O3 Layers during Lithiation-Delithiation Cycles. *Nano Lett.* **2011**, *11*, 4188−4194.
(58) Glass, A. M.; Nassau, K. Lithium ion conduction in rapidly quenched Li2O-Al 2O3, Li2O-Ga2O3, and Li2O-Bi2O3 glasses. *J. Appl. Phys.* **1980**, *51*, 3756−3761.
(59) Specht, M.; Städele, M.; Jakschik, S.; Schröder, U. Transport Mechanisms in Atomic-Layer-Deposited Al2O3 Dielectrics. *Appl. Phys. Lett.* **2004**, *84*, 3076−3078.
(60) Caglar, M.; Ilican, S.; Caglar, Y.; Yakuphanoglu, F. Electrical Conductivity and Optical Properties of ZnO Nanostructured Thin Film. *Appl. Surf. Sci.* **2009**, *255*, 4491−4496.
(61) Brook, R. J.; Yee, J.; Kröger, F. A. Electrochemical Cells and Electrical Conduction of Pure and Doped Al2O3. *J. Am. Ceram. Soc.* **1971**, *54*, 444−451.
(62) Maintz, S.; Deringer, V. L.; Tchougréeff, A. L.; Dronskowski, R. LOBSTER: A Tool to Extract Chemical Bonding from Plane-Wave Based DFT. *J. Comput. Chem.* **2016**, *37*, 1030−1035.
(63) Yoon, C. S.; Jun, D.-W.; Myung, S.-T.; Sun, Y.-K. Structural Stability of LiNiO2 Cycled above 4.2 V. *ACS Energy Lett.* **2017**, *2*, 1150−1155.
(64) Myung, S.-T.; Izumi, K.; Komaba, S.; Yashiro, H.; Bang, H. J.; Sun, Y.-K.; Kumagai, N. Functionality of Oxide Coating for Li[Li0.05Ni0.4Co0.15Mn0.4]O2 as Positive Electrode Materials for Lithium-Ion Secondary Batteries. *J. Phys. Chem. C* **2007**, *111*, 4061−4067.
(65) Li, J.; Xiao, X.; Cheng, Y.-T.; Verbrugge, M. W. Atomic Layered Coating Enabling Ultrafast Surface Kinetics at Silicon Electrodes in Lithium Ion Batteries. *J. Phys. Chem. Lett.* **2013**, *4*, 3387−3391.
(66) Asano, T.; Sakai, A.; Ouchi, S.; Sakaida, M.; Miyazaki, A.; Hasegawa, S. Solid Halide Electrolytes with High Lithium-Ion Conductivity for Application in 4 V Class Bulk-Type All-Solid-State Batteries. *Adv. Mater.* **2018**, *30*, 1803075.
(67) Arbi, K.; Rojo, J. M.; Sanz, J. Lithium Mobility in Titanium Based Nasicon Li1+xTi2-xAlx(PO4)3 and LiTi2-xZrx(PO4)3 Materials Followed by NMR and Impedance Spectroscopy. *J. Eur. Ceram. Soc.* **2007**, *27*, 4215−4218.
(68) Deng, Y.; Eames, C.; Fleutot, B.; David, R.; Chotard, J.-N.; Suard, E.; Masquelier, C.; Islam, M. S. Enhancing the Lithium Ion Conductivity in Lithium Superionic Conductor (LISICON) Solid Electrolytes through a Mixed Polyanion Effect. *ACS Appl. Mater. Interfaces* **2017**, *9*, 7050−7058.
(69) Xiao, Y.; Miara, L. J.; Wang, Y.; Ceder, G. Computational Screening of Cathode Coatings for Solid-State Batteries. *Joule* **2019**, *3*, 1252−1275.

https://dx.doi.org/10.1021/acsami.0c10000
ACS Appl. Mater. Interfaces XXXX, XXX, XXX−XXX